ISSN 0915-633X

NATIONAL INSTITUTE FOR FUSION SCIENCE

Energy Confinement Scaling from the International Stellarator Database

U. Stroth, M. Murakami, R.A. Dory, H. Yamada,
S. Okamura, F. Sano and T. Obiki

(Received - Aug. 25, 1995)

NIFS-375 Sep. 1995

RESEARCH REPORT
NIFS Series

NAGOYA, JAPAN

Energy Confinement Scaling from the International Stellarator Database

U. Stroth

Max-Planck-Institut für Plasmaphysik, Garching, Germany

M. Murakami, R. A. Dory

Oak Ridge National Laboratory, Oak Ridge, USA

H. Yamada, S. Okamura

National Institute for Fusion Science, Nagoya, Japan

F. Sano, T. Obiki

Plasma Physics Laboratory, Kyoto University, Uji, Japan

An international stellarator database on global energy confinement is presented comprising data from the ATF, CHS and Heliotron E heliotron/torsatrons and the W7-A and W7-AS shearless stellarators. Regression expressions for the energy confinement time are given for the individual devices and the combined dataset. A comparison with tokamak L mode confinement is discussed on the basis of various scaling expressions. In order to make this database available to interested colleagues, the structure of the database and

the parameter list are explained in detail. More recent confinement results incorporating data from enhanced confinement regimes such as H mode are reported elsewhere.

keywords: stellarator, heliotron/torsatron, energy confinement time, scaling, database

1.. Introduction

Scaling expressions for the global energy confinement time are widely used for both predicting the performance of future devices and comparing the quality of discharges collected from existing experiments. They are deduced from databases for global plasma parameters collected from different devices. The most comprehensive sets of tokamak data are stored in the ITER L and H mode global confinement databases [1–3].

Up to now, predictions and comparisons of stellarator performance have mostly been done on the basis of the empirical LHD scaling expression [4], deduced from a limited number of data, or on the basis of the semi-empirical Lackner-Gottardi expression [5]. We now present a more comprehensive dataset for the analysis of stellarator confinement, comprising data from the ATF, CHS, Heliotron E, W7-A and W7-AS stellarators. The term *stellarator* is used for the magnetic confinement concept with an external coil system, which includes heliotron/torsatron devices, conventional stellarators in the narrow terminology and advanced stellarators.

As in the case of tokamaks, the analysis of this database is carried out on the assumption that confinement in all the devices is goverend by similar physics processes. The devices in this paper differ most notably in the profile of the rotational transform ι, and therefore in the magnetic shear. The ι profiles of the different heliotron/torsatron devices, ATF, CHS and Heliotron E, are similar. The rotational transform ι increases strongly to the plasma edge, where one has a - similar but radially inverse to tokamaks - region of strong magnetic shear together with low-order rational numbers of ι. In contrast, the W7-A and W7-AS shearless stellarators have very flat ι profiles. Further differences are the fraction of trapped particles and the magnetic hill present in the edge region of heliotron/torsatron

plamas. However, the devices may also differ in the way they are operated.

One of the intriguing questions is whether and how heliotron/torsatron devices and shearless stellarators can be cast into one unique scaling expression. Besides the average minor (a) and the major radii (R) of the last closed flux surface, a configuration-dependent parameter (s) will therefore be used to describe differences in confinement of the two lines of stellarators. Furthermore, the parameters of the line-averaged density ($\bar{n}_e$), total absorbed heating power (P_{tot}) and magnetic field strength (B_t) will be used in the regression analyses.

In the currentless stellarators, the edge rotational transform ι_a will be the equivalent of the plasma current used in tokamaks. Shaping parameters such as elongation and triangularity will not be used. The shape of stellarator plasmas changes periodically with the toroidal angle and will only enter via the volume V, which defines the minor plasma radius by $V = 2\pi^2 a^2 R$.

The paper is organized as follows: In Sec. 2, the structure of the database and the ranges of the collected data are described. In Sec. 3, a concise description of the contributing devices is given. The database is analyzed for the global energy confinement time of every single device in Sec. 4 and for the combined dataset in Sec. 5. A comparison with tokamak confinement is added in Sec. 6. In the Appendices the parameter descriptions (A) and the data selection used for the scaling studies (B) are given.

2.. Overview of the database

The database contains electron-cyclotron-resonance-heated (ECH) and neutral-beam-injection (NBI)-heated discharges from the ATF, CHS and Heliotron E heliotron/torsatrons

and the W7-A and W7-AS shearless stellarators. A total of 859 observations are stored in the database, each consisting of data for 56 parameters as detailed in Appendix A. In stellarators, a variety of enhanced confinement modes exist. Discharge phases in enhanced confinement modes such as the re-heat mode [6] or the H mode [7,8] are not included in the database. The confinement mode represented here is referred to as L mode.

The units throughout this paper are: a and R in m, density in 10^{19} m^{-3}, power in megawatts, magnetic field in tesla and confinement time in seconds. In Tables 1 and 2 a parametric overview of the database is given. In Tab. 1, the devices are characterized by their geometrical parameters and the rotational transform. CHS is the only device having a major radius clearly different from 2 m. Therefore, the R or aspect-ratio scaling will be determined mainly by CHS against all other devices. ATF will be important for the minor radius scaling in the heliotron/torsatron line and a comparison of ATF and Heliotron E will give information about the scaling with ι. For W7-AS, data from limiter and ι scans are available. Therefore, the dependences of τ_E on a and ι can also be studied in a single device.

The ι profile of the devices is very different. For the heliotron/torsatron devices the radial profile can be parametrized by the central and edge ι values by using a parabolic form (ρ is the normalized plasma radius):

$$\iota(\rho) = \iota_a + (1 - \rho^\gamma)(\iota_0 - \iota_a), \tag{1}$$

with $\gamma = 2$, 3 and 4 for ATF, CHS and Heliotron E, respectively. The parameter $\gamma = 2$ was also used for the shearless stellarators. Although the profiles do not strictly follow this function, it is precise enough for the use of the database. In the regressions, the rotational transform ($\iota_{2/3}$) at $\rho = 2/3$ is used instead of the edge value, because, if a

local transport model is assumed, a value in the confinement region is more relevant for confinement than the central or edge value. A radially weighted average of ι would be the appropriate one to use. But since a universal radial weighting function is not known, such a sophisticated procedure would not reduce the ambiguity.

The standard set used in the regressions consists of 812 discharges. In comparison with the total set, helium discharges, statistical outliers and discharges with very high power density are removed. The selection of the standard set is described in Appendix B.

For the analyses, a further assumption is that the different heating methods can be treated on an equal footing. In Tab. 2, statistical details of the parameters of discharges from different devices and heating methods are given. The ranges in density and total absorbed heating power exceed a factor of 10. Because of the resonance condition of ECH, all devices are operated basically at two values for the magnetic field which differ by a factor of two. In this case, the average value is only of interest for the statistical analysis.

A peculiarity of the dataset is that the density ranges of ECH and NBI discharges are almost separated. This is due to the density cut-off of ECH. Only in W7-AS, where a gyrotron at 140 GHz is operated, are ECH discharges at higher densities available. The scaling expressions describe ECH and NBI discharges with similar quality. A bias might, however, be introduced by the fact that there is a majority of NBI discharges for heliotron/torsatrons and a majority of ECH discharges for the shearless stellarators.

3.. Individual Device Descriptions

In the following the different devices are described and the discharges selected for this database are characterized.

3.1.. *ATF*

ATF is an l=2/m=12 torsatron with $t_0 = 0.3$, $t_a = 1$ and $B_t \leq 2$ T [9]. The total number of datasets included in the database is 237, taken between 1988 and 1991 [10–13]. In order to accumulate radial profiles, most datasets come from sequences of typically 3 to 20 discharges under nominally identical plasma conditions. Values of the global parameters were those averaged over these discharge sets nominally at the stationary conditions.

The data included in the database are mostly data taken in the standard geometry with $R = 2.1$ m and $a = 0.27$ m. Only a few are from a radial scan where R was varied by 10%. The outermost flux surface is defined to be at the $\iota = 1$ radius in the vacuum geometry. This flux surface is usually not in contact with the wall. The magnetic field was varied from 0.6 to 1.9 T. Heating sources were ECH alone for 53 discharges (with $\bar{n}_e$ between 0.1 and $1 \times 10^{19}\mathrm{m}^{-3}$); ECH and NBI overlapping for 52 (with $\bar{n}_e$ up to $5 \times 10^{19}\mathrm{m}^{-3}$) and NBI alone for 127 discharges (with $\bar{n}_e$ up to $11 \times 10^{19}\mathrm{m}^{-3}$). Since the ECH power monitor data suffered from temporal variations, time and shot averages were supplied to the database. Essentially 100% of the ECH port-through power was considered to be absorbed in the plasmas [14]. NBI power was re-evaluated (with in-situ measurements), with the maximum power injected being 1.4 MW with co and counter tangential injectors.

3.2.. *CHS*

The Compact Helical System (CHS) is an l=2/m=8 heliotron/torsatron with an aspect ratio of as low as 5 [15]. Data from 197 discharges in the standard configuration are stored in the database. The data were taken between 1989 and 1993. The standard

configuration is defined by the following conditions: the magnetic axis is at 0.92 m, the toroidally averaged plasma elongation is 1.12. The stored energy as well as the central electron temperature has shown a significant dependence on the magnetic axis position [16]. The dataset included is an optimal case of an inward shifted geometry with respect to the major radius of the helical coils. The plasma boundary is well defined by the inner wall (stainless steel) of the vacuum chamber which works as a limiter in this configurational set-up. The wall was conditioned by titanium gettering for all cases. Improved modes [6,8], which enhance the confinement as much as 30%, have not been included in the database. The chosen time slices are close to steady state with $\dot{W} < 0.03\ P_{tot}$.

Although NBI in CHS (<1.1 MW, 40 keV) has the capability to change the injection angle [17], the present data are limited to tangential co-injection. The NBI power deposition is estimated by an interpolating expression deduced from HELIOS Monte Carlo simulations [18,19]. The validity of this model was checked by comparing the experimental magnetic axis shift and the diamagnetic measurements with MHD calculations corrected by the calculated beam pressure [20].

The description of the magnetic geometry is based on computations with the VMEC code [21]. The diamagnetic stored energy includes a certain amount of beam pressure. Its contribution reaches 30% when the electron density is as low as $1 \times 10^{19}\mathrm{m}^{-3}$ and decreases to less than 10% when the electron density exceeds $5 \times 10^{19}\mathrm{m}^{-3}$. Because of the low aspect ratio, the orbits of the tangetially injected fast ions significantly deviate from the magnetic surfaces. Even fast particles born in the core region can therefore suffer from charge-exchange losses occurring closer to the plasma edge. Because of longer slowing-down times, this loss mechanism is enhanced in low-density operation. Also the

shine-through is larger at low densities. Consequently, the deposited power from NBI has a strong correlation with the electron density.

On the basis of the radiation level at the plasma collapse, ECH (53 GHz, < 200 kW) power deposition is assumed to be 70% of the port-through power.

3.3.. Heliotron E

Heliotron E is an l=2/m=19 heliotron with a large rotational transform and strong magnetic shear [22]. Its contribution to the database consists of 121 time slices from both ECH-only (<0.5 MW) and NBI-only (<4 MW) currentless plasmas, taken from the period of 1985 to 1993. For each plasma discharge, the stationary phase was chosen to determine the plasma profiles. The magnetic configuration was fixed to the standard configuration with R = 2.17 m, a radius of the magnetic axis of 2.2 m and a = 0.21 m. The ratio of the vertical and toroidal magnetic field strengths was fixed at B_v/B_t = -0.185 without the additional toroidal field coils energized. The toroidal magnetic field on axis was mainly 0.94 and 1.9 T due to the given gyrotron frequency of 53 GHz.

The injection angles of the three neutral beam lines are all near-perpendicular. Data for H beam into H plasma and H beam into D plasma are included in the database. The estimation of the absorbed beam power is based on the HELIOS Monte Carlo code [19]. In most cases, however, the PROCTR-mod code and an empirical estimate of the orbit losses as derived from HELIOS were combined [23,24]. The validity of this approach was confirmed by full HELIOS code calculations. The port-through power was experimentally determined by using the calorimeter system of each beam line.

Earlier analyses of the global confinement time or the electron thermal diffusivity for

NBI plasmas suggested that the anomalous transport in the outer plasma region closely followes a gyro-reduced-Bohm-type of scaling [24]. The presently selected data are an extension of these data.

For ECH plasmas, the absorbed power was determined from the decay of the electron temperature profile after ECH power turn-off. About 60-70% of the port-through power was determined by this procedure [25,26].

The line-averaged electron density is provided by multi-channel FIR combined with Thomson scattering data. The ion temperature profile was determined by a neutral particle analyzer, but the edge temperature was corrected by the neoclassical prediction and, in some cases, by charge exchange spectroscopy data.

For all plasma discharges, the thermal plasma energy content was determined from the profile (kinetic) measurements. In some cases, these kinetically determined values were compared with the diamagnetic values showing reasonable agreement [27]. The regression analyses use the thermal confinement time as determined from the profiles.

The majority of discharges were separatrix-limited discharges in the natural divertor configuration with titanium-gettered stainless-steel wall. The coverage of the gettering on the vessel surface was typically 30 to 40% of the total surface. It should be noted, however, that some of the NBI discharges were done in a carbonized vessel (in order to achieve high density) and the discharges in 1993 in a boronized one (in order to control recycling and impurity content).

Finally, it is important to note that the Heliotron E confinement can be improved by 20 to 30% in relation to the standard configuration included in this database, if the magnetic axis is shift inward by about 2 cm [27].

3.4.. W7-A

Wendelstein 7-A (W7-A) was a classical l=2/m=5 stellarator with $R = 2$ m, $a = 0.12$ m and a low shear rotational transform profile [28]. Although operation was possible both with and without a net plasma current, the best confinement performance was observed in operation without net plasma current [29–31]. The 13 datasets contributing to the database were from operation without plasma current and, as in W7-AS, at ι values with optimum plasma confinement. The boundary of the elliptically shaped plasma was determined by a molybdenum limiter at $a \simeq 0.1$ m. Only ECH discharges are included in the database, taken at two values of the rotational transform and at $B_t = 1.25$ and 2.5 T.

3.5.. W7-AS

Wendelstein 7-AS (W7-AS) is an advanced modular stellarator with a partially optimized magnetic configuration to minimize the Pfirsch-Schlüter currents [32–34].

The total number of datasets included is 291, taken between 1992 and 1994. During and before this period, frequent boronization was applied to the vacuum vessel. It is important to note that, during the consecutive boronization of the vessel, the diamagnetic confinement time has improved successively with an overall improvement of about 15% over the previous data [35].

All discharges were carried out in the standard configuration at optimum confinement. The standard configuration is defined as $R = 2.05$ m and B_t mostly 1.25 or 2.5 T with the same coil current running through all modular coils. At low β, confinement in W7-AS depends in a complicated way on the rotational transform [34]. The optimum confinement properties are obtained in the vicinity of $\iota = \frac{1}{3}$ and $\frac{1}{2}$. At other values, confinement is

deteriorated, possibly by major rational ι values being inside the confinement region. The magnetic shear of the vacuum field is small. An ohmic transformer is used to balance beam-driven and bootstrap currents. Although the total net current is reduced to values below 100 A, the residual local current density modifies the shear profile to some extent.

At $\iota = \frac{1}{3}$, the last closed flux surface is determined by two limiters, situated at the top and bottom of the plasma. In the database, data are included where a was changed from 0.11 to 0.18 m by moving the limiters. At $\iota = \frac{1}{2}$ and the largest limiter aperture, the plasma boundary is determined by natural islands. But in this configuration too, discharges are included with the limiters moved inside the plasma.

Much care has been taken to select the data so as to fill the plasma parameter space uniformly. Since the plasma parameters in NBI experiments are restricted by a smaller variation in heating power and by collinearities between power and density, only a smaller number of NBI discharges are present in the database. The selected data are consistent with the W7-AS confinement properties as published in [36–39].

Heating sources were ECH alone for 198 discharges, ECH and NBI overlapping for 7 discharges and NBI alone for 45 discharges. It was assumed that 90% and 100% of the measured port-through power has been absorbed in first and second harmonic ECH, respectively. Data from heating with both the 70 and the 140 GHz gyrotrons are included. NBI is near tangential. For the absorbed NBI power an approximation formula is used which relies on Fafner Monte Carlo code [40] calculations, taking into account shine-through, orbit losses and secondary charge exchange.

4.. Analyses of Data from the Individual Devices

In this section, the properties of the individual datasets are discussed. In Tab. 3, the correlation between the plasma parameters of the standard set is shown for the devices. The dataset of W7-A is too small for an individual analysis and is omitted here. A common feature of all datasets is the rather strong correlation between density and heating power. Beam fuelling and neutrals desorbed from the walls increase with increasing heating power. In addition, at low densities, charge exchange and shine-through losses decrease with increasing density. Higher plasma density operation is possible at high NBI power.

This correlation can be weakened to some extent by ECH discharges, in which particle control is much easier to achieve. Consequently, one finds the strongest correlation of 95% in CHS with the lowest relative number of ECH discharges in the dataset. For the datasets with a strong correlation, the dependence of τ_E on $\bar{n}_e$ and P_{tot} cannot be determined independently with sufficient accuracy.

In the analysis of single devices, the dependence of τ_E on a and ι can only be deduced from W7-AS. This device is represented by a dataset with the strongest correlation being 64% between density and power. Also the ATF dataset shows rather low correlation between B_t and the other plasma parameters.

In Tab. 4, results of linear regression analyses are listed for the individual machines. In all cases use is made of an ansatz of the form

$$\tau_E = 10^{\alpha_z} a^{\alpha_a} R^{\alpha_R} P_{tot}^{\alpha_P} \bar{n}_e^{\alpha_n} B_t^{\alpha_B} \iota_{2/3}^{\alpha_\iota} \,. \tag{2}$$

The total absorbed heating power P_{tot} is the sum of absorbed ECH and NBI powers. Parameters which cannot be determined from the individual datasets have been fixed at

the values underlined in the table.

The database does not give a clear picture of the dependence of τ_E on the plasma isotopic mass. Because of the lack of D beam into D plasma injection data, the isotopic effect cannot be investigated for NBI discharges. A small positive isotopic effect is indicated for ECH discharges of ATF and Heliotron E. But the dataset does not show a dependence on the isotopic mass. A mass dependence has not been further pursued in the analyses.

The general trends documented in Tab. 4 are similar for all devices: the energy confinement time strongly improves with magnetic field and density and degrades with heating power. Besides CHS, which may suffer from the strong correlation between $\bar{n}_e$ and P_{tot}, the parameters of the single-device regressions overlap in almost all combinations within one standard deviation. An exception is the weak B_t dependence found for Heliotron E. The Heliotron E dataset also shows the strongest correlation between B_t on the one hand and $\bar{n}_e$ and P_{tot} on the other.

CHS, in contrast, shows a rather strong dependence on B_t. If α_P is constrained to -0.6, a fit with similar quality is found with an $\bar{n}_e$ dependence like $\alpha_n = 0.47$, but the B_t dependence still remains strong.

Excellent agreement is found between the parameter dependences of ATF and W7-AS, the two devices with the lowest correlation in the datasets. This is encouraging in view of a description of the entire dataset by a unique scaling expression. From W7-AS alone, a close to quadratic dependence of τ_E on the plasma radius is found as well as a distinct improvement with the rotational transform.

The data also indicate that the density dependence of τ_E might be more complicated than a simple power law. The dependence seems to be stronger at low densities and weaker

at high ones. A saturation of τ_E with density at the highest densities, similar to that in the saturated ohmic confinement regime in tokamaks, cannot be ruled out. Therefore, it is strongly recommended that the scaling expressions not be used for densities beyond $10^{20}\mathrm{m}^{-3}$, the range well covered by this database. Only 3% of the discharges are at higher densities. Up to this density, the expressions describe the average trend in the data well.

5.. Inter-Machine Regression Analyses

For the analysis of the combined dataset, two major assumptions must be made: (i) the dependences of τ_E on plasma parameters which can be readily varied in the individual machines, like P_{tot}, $\bar{n}_e$ and B_t, must be similar for all devices and (ii) the confinement of ECH and NBI discharges must follow the same scaling expressions. Only under these assumptions do the data of the five devices included in this database contain sufficient information to deduce the dependences of τ_E on the configuration parameters, such as a, R and ι.

Table 5 illustrates the importance of particular devices in extracting specific parametric dependences. It summarizes the information on the a, R and ι dependences obtained from comparisons of subsets of devices. Since the main interest here is the dependences on the device-specific parameters, the parameters α_P, α_n and α_B were in some cases fixed to the values obtained from single-device regressions (see Tab. 4).

As mentioned earlier, W7-AS alone gives information about the a and ι dependences (no. 1 in Tab. 5). Assuming an R dependence similar to that found for the heliotron/torsatron line, one gets the expression

$$\tau_E = 0.115 \times a^{2.21} R^{0.74} P_{tot}^{-0.54} \bar{n}_e^{0.50} B_t^{0.73} \iota_{2/3}^{0.43} \,. \tag{3}$$

If the W7-A and W7-AS datasets are combined (no. 2), the α_a parameter increases from 2.21 to 2.27. On the assumption that a similar a scaling also applies to the heliotron/torsatron line, the datasets of ATF and CHS (no. 3) can be unified by an R scaling like $\alpha_R = 0.81$. Hence, the confinement time increases almost linearly with the plasma volume. In this regression, imposing a weaker a dependence leads to a stronger R dependence.

The combined dataset of ATF and Heliotron E (no. 4) may give information about the ι dependence in the heliotron/torsatron line. With $\alpha_\iota = 0.36$ it turns out to be close to the value found for W7-AS ($\alpha_\iota = 0.43$). This result might depend on how the ι value is chosen. In order to get an idea of the importance of the choice of the ι value, regression analyses were carried out, using ι values from different radial positions. The result is that the regression parameters alter to $\alpha_\iota = 0.45$ and 0.23 if ι is taken at $\rho = \frac{1}{3}$ and 1, respectively.

Combining all three heliotron/torsatrons (no. 5) yields a complete scaling expression with the parameter dependences being very close to the parameters found for W7-AS alone (ι at $\rho = \frac{2}{3}$ being used again here):

$$\tau_E = 0.0398 \times a^{2.06} R^{0.74} P_{tot}^{-0.63} \bar{n}_e^{0.53} B_t^{0.80} \iota_{2/3}^{0.39} \ . \tag{4}$$

It is an encouraging result that the data of the heliotron/torsatron line is consistent with the parameter dependences found for W7-AS. Omitting ι as a regression variable significantly modifies the dependences on a and R:

$$\tau_E = 0.0132 \times a^{1.51} R^{1.04} P_{tot}^{-0.62} \bar{n}_e^{0.53} B_t^{0.81} \ . \tag{5}$$

The small increase of the rmse from 0.0902 to 0.0909 by omitting ι as a regression variable is statistically significant. However, it should be noted that the ι and aspect ratios are

closely related in heliotron/torsatron devices. A variety of theories indicate that the transport and MHD stability characteristics significantly change with aspect ratio. Therefore it should not necessarily be concluded here that the iota value directly affects confinement in heliotron/torsatron devices.

The next question is how to derive a single unified expression for all devices. For this purpose, we introduce one additional parameter (s) in the form

$$\tau_E = 10^{\alpha_x} 10^{s\alpha_s} a^{\alpha_a} R^{\alpha_R} P_{tot}^{\alpha_P} \bar{n}_e^{\alpha_n} B_t^{\alpha_B} t_{2/3}^{\alpha_t} \,. \tag{6}$$

The parameter assumes the value $s = 1$ for heliotron/torsatrons and $s = 0$ for shearless stellarators. It could represent differences in the configurations (shear, trapped particle fraction, magnetic well/hill) as well as cleanness of the devices or efforts at optimization.

In Tab. 6, the regression expressions obtained from the entire standard set are summarized. The unconstrained fit (no. 1) is in good agreement with the experience gathered so far. The confinement data from three heliotron/torsatrons and two shearless stellarators can be unified if the parameter s is taken into account. The dependences on the other parameters are consistent with the results obtained from heliotron/torsatrons and shearless stellarators separately. In Fig. 1 the the quality of the fit can be seen.

When the s parameter is not introduced, the regression results in expression no. 2. The fit gives a weaker dependence on the minor radius and a larger root-mean-square error. The parameter dependences are close to the one of the t-independent scaling in Eq. 5. There are two different ways of analyzing the combined dataset: (i) by introducing the configuration-specific parameter s , leading to an t dependence of the confinement time, or (ii) by deducing an expression without introducting s, yielding a very weak t dependence at the expense of a larger rmse.

Expression no. 3 gives a dimensionally correct fit to the data which has the same rmse as the unconstrained one. It was obtained by imposing the additional constraint [42]

$$3\alpha_P + 8\alpha_n + 5\alpha_B - 4(\alpha_a + \alpha_R) + 5 = 0. \tag{7}$$

The magnetic configurations of the two stellarator lines differ in many respects (number of trapped particles, magnetic well and shear). These differences are accounted for in a rather crude way by the parameter s and it is difficult to relate the value of α_s to a unique physical parameter. Furthermore, α_s is influenced by possible systematic differences in the datasets of the two stellarator lines. For this reason, we propose as International Stellarator Scaling (ISS) the expression

$$\tau_E^{ISS95} = 0.079 \times a^{2.21} R^{0.65} P_{tot}^{-0.59} \bar{n}_e^{0.51} B_t^{0.83} \iota_{2/3}^{0.4} \,. \tag{8}$$

The expression has the same parameter dependences as no. 3, but the pre-factor has been adjusted to be in the centre between the heliotron/torsatron and shearless stellarator confinement. In Sec. 3.5 it was mentioned that, due to clean vessel conditions, the confinement of the W7-AS data in the database is improved by 15% in relation to a previous dataset. To test the influence of such an effect on the results, a regression was carried out where τ_E of W7-AS was artificially reduced by 15%. The result given in Tab. 6 (no. 4) indicates that with $\alpha_s = -0.21$ the configuration-dependent variable is still necessary to improve the fit.

The size of the W7-AS plasma is determined by only two limiters. This leads in the average to long connection lengths of field lines interacting with limiters. The length is even more increased in relation to heliotron/torsatrons because of the low ι value in W7-AS. The long connection length in W7-AS could lead to poloidal asymmetries in density

and temperature in the scrape-off layer and therefore to a virtually larger plasma radius. Such an effect was simulated by increasing the minor plasma radius of W7-AS artificially by the large amount of 20%. The result of this regression is given under no. 5. Although α_s = -0.08 still indicates some configuration dependence, a larger effective minor radius of W7-AS would modify the conclusions of this work.

It was also tested whether the choice of the radial position at which the ι value is taken influences the results. Regressions using ι at $\rho = \frac{1}{3}$ or 1 do not, however, qualitatively change the results.

No distinct difference between ECH and NBI can be diagnosed. Because of the different density ranges in the two heating methods, a possible difference might, however, be hidden in the density scaling properties.

6.. Comparison with Tokamak L Mode Confinement

After the comparison between shearless stellarators and heliotron/torsatron devices it is now tempted to include tokamaks as well. The toroidal plasma current will enter this study only as a source of the poloidal magnetic field, which determines $\iota = 1/q$. The stellarator database is compared with tokamak L mode data using the ITER L mode database. The bases for the comparison will be the Lackner-Gottardi (L-G) [5], the LHD [4] and the ISS95 expressions. The definition of ι or q used in the scaling expressions must be consistent. For the LHD expression, which does not depend on ι, this is not important:

$$\tau_E^{LHD} = 0.034 \times a^2 R^{0.75} P_{tot}^{-0.58} \bar{n}_e^{0.69} B_t^{0.84} \,. \tag{9}$$

Scaling expressions for tokamak confinement are expressed in terms of the plasma current I_P. For comparison with stellarators, they have to be rephrased by using (I_P in MA)

$$I_P = 5\frac{a^2 B_t}{R}\frac{1+\kappa^2}{2}\iota. \tag{10}$$

The crucial question in these comparisons is the radius at which ι should be evaluated. If the edge ι values were used, the scaling would predict an improvement in confinement of a factor of about 3 from a comparable $q = 5$ tokamak to Heliotron E with $\iota_a = 2.8$. Since confinement is not produced exclusively at the plasma edge, this is not realistic and the use of $\iota_{2/3}$ seems more appropriate. Equivalently, current-ramp experiments in tokamak [43] indicating that confinement increases with a radial peaking of the plasma current profile also suggest that not the total plasma current but rather the current flowing inside some smaller radius is relevant to confinement.

For the calculation of $\iota_{2/3}$ for tokamaks we use a radial q profile of the form

$$q(\rho) = \frac{\rho^2}{1-(1-\rho^2)^4} q(\rho = 1)\,. \tag{11}$$

A further difference occurs in the definition of the minor plasma radius. For stellarators, it is defined via the plasma volume ($V = 2\pi^2 a^2 R$) and in tokamaks with an elliptical elongation κ by the minor half-axis of the ellipse ($V = 2\pi^2 a^2 \kappa R$ if triangularity and indentation are neglected). Since τ_E depends about quadratically on a, it will be crucial for the comparison to use the appropriate value. If stellarator data are used in a tokamak scaling expression, $a/\sqrt{\kappa}$ should be inserted instead of a. And if tokamak data are used in the stellarator expressions of this paper, $a\sqrt{\kappa}$ has to be used.

The elongation in a 3-dimensional plasma changes with toroidal angle and κ is not entered in the stellarator database. Hence, a comparison with the ITER89-P scaling is

not possible. But a sensible comparison can be done on the basis of the L-G expression, where τ_E scales with $a^2\kappa$. In this case it is consistent to use $\tau_E \sim a^2\kappa$ for tokamaks and $\tau_E \sim a^2$ (with $\kappa = 1$) for stellarators. The L-G expression [5] in stellarator notation reads

$$\tau_E^{L-G} = 0.68 \times 0.0627 \times a^2 R P_{tot}^{-0.6} \bar{n}_e^{0.6} B_t^{0.8} \diamond$$

B3=œ(Jiotabar$_{2/3}^{0.4}$.(12)The term $\left(\frac{1+\kappa^2}{1+\kappa}\right)^{0.8}$ was neglected here. The pre-factor 0.68 has been obtained by adjusting the scaling expression to the centre of gravity of the combined stellarator-tokamak dataset. Since we use $\iota_{2/3}$ instead of $\iota(a)$, this adjustment was necessary.

A comparison of stellarators and tokamaks on the basis of different scaling expressions is shown in Fig. 2. Plotted is the average of $(\tau_E - \tau^{scal})/\tau^{scal}$ over all discharges for each device using for τ^{scal} the predictions from the various scaling expressions. On the average, the LHD and L-G expressions describe both stellarators and tokamaks with similar quality. Deviations from the scaling expressions of up to 40% of the energy confinement time are observed. Similar deviations are also present if the ITER89-P [1] expression is applied to this tokamak L mode dataset. The ι dependence present in the L-G expression introduces a larger scatter for the stellarator devices. The LHD expressions reproduces almost exactly the center of gravity of the combined dataset. On the basis of the L-G expression, the quality of W7-AS confinement is similar to the average tokamak confinement. The other stellarator and heliotron/torsatron devices are on the level of the lowest tokamaks.

The ISS95 expression describes stellarators and tokamaks equally well. The scatter of the stellarators around the fit is about the same as for the tokamaks. It is a remarkable result that a scaling expression derived from small stellarators describes rather well the confinement time of a large tokamak like JET. A detailed comparison of all data with the

ISS95 expression is shown in Fig. 3.

7.. Summary and Conclusion

A new stellarator database for global plasma parameters has been presented. A total of 859 discharges are included from the devices ATF, CHS, Heliotron E, W7-A and W7-AS. In contrast to tokamaks, the devices fall into two groups distinguished by their magnetic configuration. ATF, CHS and Heliotron E are heliotron/torsatrons with strong positive magnetic shear and a radially limited magnetic well. W7-A and W7-AS are characterized by a very low shear and a magnetic well throughout the plasma cross-section.

The database covers ECH and NBI discharges. Although the heating physics of the two methods is very different, the confinement properties have to be assumed to depend only on the total absorbed heating power. The scaling expressions obtained describe ECH and NBI discharges equally well.

Regression analyses have been carried out for the individual stellarator lines as well as for the combined dataset. The heliotron/torsatron data are consistent with the expression shown in Eq. 4. If the R dependence is assumed, the shearless stellarators are described by the expression shown in Eq. 3.

For a combined analyses of the dataset it is very satisfactory that the dependences of the two individual expressions on the plasma parameters are very similar. In order to obtain an optimum fit of all devices, we introduced a parameter (s) representing the two different stellarator lines, $s = 0$ for shearless stellarators and $s = 1$ for the heliotron/torsatron line. With this parameter included in the regression, we derived two scaling expressions with very tight fits (Tab. 6, no.1 and 3), the latter satisfying Connor-Taylor-type theoretical

constraints (Eq. 7). However, the absolute value of the dependence on s also depends on the consistency of discharge conditions and parameter definitions in the two stellarator lines. The effect of the cleanness of the vessels and of different definitions of the plasma radius was discussed in Sec. 5. Also the correlation of s and ι introduces some uncertainty in the s dependence.

Besides the expressions which can be used for the individual stellarator lines, we therefore give an expression (ISS95) which disregards the s parameter and allows the confinement of the different stellarators to deviate from the fit to an extent similar to that to which tokamaks deviate from the fits (see Sec. 6):

$$\tau_E^{ISS95} = 0.079 \times a^{2.21} R^{0.65} P_{tot}^{-0.59} \bar{n}_e^{0.51} B_t^{0.83} \iota_{2/3}^{0.4} \,. \tag{13}$$

The parameter dependences are similar to those of the Lackner-Gottardi expression (Eq. 6). No dependence of τ_E on the isotopic mass is indicated in the dataset.

A comparison of stellarator and tokamak confinement has been carried out on the basis of various scaling expressions. As described in Sec. 6, it is crucial to use the appropriate definitions for a and ι in this comparison. It has been shown that Eq. 13 also describes tokamak data surprisingly well. And also on the basis of the other expressions, the stellarator and the tokamak L mode are of comparable confinement quality.

Some cautionary remarks are in order:

(1) The density dependence of τ_E turns out to be more complicated than a simple power law. A stronger dependence seems to be indicated in the low density domain and a weaker one at higher densities. In average the above expression describes the data for densities of up to 10^{20} m^{-3}. It is strongly advised not to apply this expression to densities higher than this value.

(2) The period of experimentation to acquire the data included in this database spans over ten years, and during this period substantial progress has been made in wall-conditioning techniques. Therefore there are, as in tokamak databases too, variations in discharge cleanness which might distort the scaling results.

(3) Recent results from enhanced confinement regimes such as H mode are excluded from the database.

(4) In Fig. 3, the data of heliotron/torsatron devices and shearless stellarators have opposite offsets with respect to the ISS95 scaling. It should be noted that data stored in the database are primarily obtained in each standard operation. Operational modes with better confinement are obtained by means of intense wall conditioning and tailoring the magnetic geometry in each device. The ISS95 scaling should be recognized as an L-mode-like scaling. The parameter s has been used in unifying the entire dataset. However, the physical meaning of s is not obvious. Although, it might be attributed to differences in magnetic configuration and/or experimental conditions, there are other effects which could be responsible for this as well.

The ISS95 scaling is based on the selection of the iota-dependent scaling for heliotron/torsatron confinement. If the iota-independent scaling is selected, the offsets reduces to a level similar to that when the LHD expression is used. The next generation experiments LHD and W7-X will allow to distinguish more clearly between the two scaling expression.

With the publication of this article, the database will be available for interested colleagues. We look forward to seeing future upgrades of the database.

Acknowledgements

It is a pleasure to acknowledge the encouragement received from M. Fujiwara O. Motojima and F. Wagner. Helpful discussions with O. Kardaun and H. Wobig are appreciated. We thank H. Renner for the W7-A data and S. Kaye, who supplied us with a recent version of the ITER L mode database.

Appendix A.. Parameter Description

Missing data or data which are not available are characterized by -9999999 for integers, -9.999E-09 for real and NODATA for characters.

Heating powers which are not applied are set to 0 and additional heating parameters (i.e. PGASA, FECH1...) which are not applicable are set to be "missing" (see above).

General parameters

1 **STELL** Stellarator that has supplied the data:

ATF, CHS, HELE, W7-A, W7-AS

2 **UPDATE** Last update [YYMMDD]

3 **DATE** Date on which the shot was taken [YYMMDD]

4 **SHOT** Shot number or the first shot number of a sequence

5 **SEQ** Sequence number (designated for a series of similar shots)

6 **TIME** Time during the shot at which the data are taken [s]

7 **PHASE** Phase of the discharge:

STAT = stationary phase

Plasma composition

8 **PGASA** Mass number of the plasma working gas:

1= H_2; 2= D_2; 3=He_3; 4=He_4

9 BGASA Mass number of the NBI gas:

1= H_2; 2= D_2

10 RGEO Major radius of the last closed flux surface [m]

ATF: (Rmax+Rmin)/2

Heliotron E: 2.17 m + radial displacement

W7-AS: 2 m + radial displacement

11 RMAG Major radius of the magnetic axis in the vacuum [m] geometry

Heliotron E: 2.2 m + radial displacement

W7-AS: 2.05 m + radial displacement

12 AEFF Effective minor radius [m]

ATF: the $\iota = 1$ radius, which is usually not in contact with the wall

CHS: radius limited by the inner wall

Heliotron E: radius of the last closed flux surface before the ergodic region

W7-AS: Last closed flux surface from simple formula interpolating between available configurations

13 SEPLIM Minimum distance between the separatrix and the wall or the limiter [m]

14 CONFIG Plasma configuration

STD = standard configuration

LIM/STD = standard configuration with limiter

Machine conditions

15 WALMAT Material of the vacuum vessel wall

IN = inconel

INCARB = inconel with carbon

SS = stainless steel

SSCARB = stainless steel with carbon

16 LIMMAT3 Limiter material

C = carbon

BORC = boron-carbide

SS = stainless steel

TIC = titanium-coated graphite

17 EVAP Evaporated material

C = carbonized

BOR = boronized

TI = titanium

CR = cromium

NONE = no evaporation

Magnetics

18 BT Vacuum toroidal field at RGEO [T]

ATF: calculated from coil current

19 IP Total plasma current [A]

Positive values if it increases the vacuum iota (equivalent to the direction of a tokamak current)

20 VSURF Loop voltage at plasma boundary [V]

positive values giving positive IP

21 IOTAA Rotational transform at the plasma edge (AEFF)

W7-AS: From simple formula interpolating between available configurations

22 IOTA0 Rotational transform at the plasma centre

W7-AS: From simple formula interpolating between available configurations

23 BETDIA Toroidal beta based on the diamagnetic measurement (fraction, not %)

Heliotron E: calculated by the PROCTR code

24 NEBAR Line average electron density [m^{-3}]

W7-AS: If available, from microwave interferometer, otherwise from a central HCN chord

25 DNEDT Time derivative of NEBAR [m^{-3}/s]

ATF: only steady state → set to 0

Heliotron E: only steady state → set to 0

W7-AS: only steady state → set to 0

Impurities

26 ZEFF Average plasma effective charge

27 PRAD Total radiative power as measured with bolometry [W]

Input power

28 PECH13 Port-through power for primary ECH [W]

Heliotron E: sum of 53 GHz powers

W7-AS: sum of 70 GHz powers

29 PECH2 Port-through power for secondary ECH [W]

W7-AS: sum of 140 GHz powers

30 MECH1 Mode of primary ECH:

1 = fundamental; 2 = 2^{nd} harmonic

31 MECH2 Mode of secondary ECH:

1 = fundamental; 2 = 2^{nd} harmonic

32 PABSECH Total absorbed ECH power [W]

Heliotrom E: from T_e decay

CHS: from radiation level at plasma collapse

Heliotron E: from power switch-off experiments

W7-AS: 90% and 100% absorption in first and 2^{nd} harmonic, respectively

33 ENBI1 Power-weighted neutral beam energy for the primary beams [V]

W7-AS: Sources 1+5; $1{:}\frac{1}{2}{:}\frac{1}{3}$ = 1:1:1

34 ENBI2 Power-weighted neutral beam energy for the secondary beams [V]

W7-AS: Sources 3+7; $1{:}\frac{1}{2}{:}\frac{1}{3}$ = 1:1:1

35 RTAN1 Tangency radius for the primary beams

36 RTAN2 Tangency radius for the secondary beams

37 PNBI1 Port-through NBI power for the primary beams [W]

38 **PNBI2** Port-through NBI power for the secondary beams [W]

39 **PABSNBI** Total absorbed NBI power corrected for shine-through, orbit and charge-exchange losses [W]

CHS: according to an expression deduced from HELIOS Monte Carlo calculations

Heliotron E: according to the HELIOS Monte Carlo beam orbit following code

W7-AS: according to a simple formula deduced from Fafner calculations

40 **PICH** Port-through ICRF power [W]

41 **FICH** ICRF frequency [Hz]

42 **PABSICH** ICRF absorbed power

43 **POH** Ohmic heating power [W]

Profile information

44 **NE0** Central electron density at RMAG [m^{-3}]

Heliotron E: taken from FIR

W7-AS: taken from a fit to a Thomson scattering profile

45 **TE0** Central electron temperature at RMAG [eV]

Heliotron E: taken from a fit to a Thomson scattering profile

W7-AS: taken from a fit to a Thomson scattering profile

Energies

46 **WDIA** Total plasma energy as determined by diamagnetic measurements [J]

Heliotron E: = from kinetic profiles and the beam contribution calculated by the Proctr code

47 WMHD Total plasma energy as determined from MHD equilibrium [J]

ATF: saddle loop is not calibrated, use for reference only

48 WETH Total thermal electron plasma energy [J]

W7-AS: from Thomson scattering profiles

49 WITH Total thermal ion plasma energy [J]

W7-AS: from simulation with neoclassical transport coefficients

50 WTH Total thermal plasma energy from kinetic meassurements [J]

51 WFPER Calculated total perpendicular fast ion energy [J]

52 WFPAR Calculated total parallel fast ion energy [J]

Energy confinement times

53 TAUEDIA Global confinement time based on diamagnetic measurrement [s]

TAUEDIA = WDIA/(PABSECH+PABSNBI+PABSICH+POH-dWDIA/dt)

ATF: dWDIA/dt = 0 is used

Heliotron E: perpendicular injection set to 1

W7-AS: dWDIA/dt = 0 is used

54 TAUETH Thermal energy confinement time [s]

TAUETH = WTH/(PABSECH+PABSNBI+PABSICH+POH-dWTH/dt)

ATF: dWDIA/dt = 0 is used

Heliotron E: dWDIA/dt = 0 is used

W7-AS: dWDIA/dt = 0 is used

Extra information

55 COFRANBI Ratio of co-injected beam port-through power to total NBI power

Heliotron E: perpendicular injection is set to 1

W7-AS: Sources(5+6+7+8)/all sources ($B_t > 0$)

56 STDSET Standard data set

0 = not included

1 = included in present analyses

Appendix B.. Selection of the Standard Set

The standard data set used in all regressions of this paper can be obtained from the entire database under the following conditions:

1. Delete discharges in helium.
2. For ATF, delete discharge no. 6842.
3. For Heliotron E, delete discharges no. 53705.
4. For W7-AS, delete all discharges with high power density given by the condition $P_{abs}/\bar{n}_e \geq 3 \times 10^{14} W\mathrm{m}^3$.
5. For W7-AS, delete discharges no. 21089, 24734, 25966, 25969, 26000 and 26925.
6. Use the diamagnetic energy confinement time; only for Heliotron E, must the thermal confinement time be used.

For observations included in the standard set, the parameter STDSET is set to 1. Otherwise this parameter is set to 0.

References

[1] YUSHMANOV, P. N., TAKIZUKA, T., RIEDEL, K. S., KARDAUN, O. J. W. F., CORDEY, J. G., et al., Nucl. Fusion **30** (1990) 1999.

[2] CHRISTIANSEN, J. P., DeBOO, J., KARDAUN, O. J., KAYE, S. M., MIURA, Y., et al., Nucl. Fusion **32** (1992) 291.

[3] ITER H-Mode Database Working Group, THOMSON, K., CAMPBELL, D. J., CORDEY, J., KARDAUN, O., RYTER, F., STROTH, U., KUS, A., DeBOO, J. C., SCHISSEL, D. P., MIURA, Y., SUZUKI, N., MORI, M., MATSUDA, T., TAMAI, H., TAKIZUKA, T., ITOH, S. I., ITOH, K., and KAYE, S. M., Nucl. Fusion **34** (1994) 131.

[4] SUDO, S., TAKEIRI, Y., ZUSHI, H., SANO, F., ITOH, K., et al., Nucl. Fusion **30** (1990) 11.

[5] LACKNER, K. and GOTTARDI, N. A. O., Nucl. Fusion **30** (1990) 767.

[6] MORITA, S., YAMADA, H., IGUCHI, H., ADATI, K., AKIYAMA, R., et al., The role of neutral hydrogen in CHS plasmas with reheat and collapse, and comparison with JIPP T-IIU tokamak plasmas, in *Plasma Physics and Controlled Fusion Research (Proc. 14th Int. Conf., Würzburg, 1992), Vol. 2, IAEA, Vienna*, pages 515–521, 1993.

[7] ERCKMANN, V. et al., Phys. Rev. Lett. **70** (1993) 2086.

[8] TOI, K. et al., Formation of an H-mode-like transport barrier in the CHS heliotron-torsatron, in *Plasma Physics and Controlled Fusion Research (Proc. 14th Int. Conf.,*

Würzburg, 1992), Vol. 2, IAEA, Vienna, pages 461–468, 1993.

[9] LYON, J. F. et al., Fusion Technol. **10** (1986) 179.

[10] DORY, R. et al., Comments Plasma Phys. Controlled Fusion **14** (1991) 237.

[11] MURAKAMI, M. et al., Energy confinement and bootstrap current studies in the advanced toroidal facility, in *Plasma Physics and Controlled Fusion Research (Proc. 13th Int. Conf., Washington, DC, 1990), Vol. 2, IAEA, Vienna*, page 455, 1991.

[12] MURAKAMI, M. et al., Phys. Fluids **B3** (1991) 2261.

[13] ISLER, R. C. et al., Phys. Fluids **B4** (1992) 2104.

[14] MURAKAMI, M. et al., Confinement studies in ECH plasmas in ATF, in *Proc. 9th Top. Conf. Radio Frequency Power in Plasmas, Charleston, NC, 1991, AIP, NY Proc. 244*, page 3, 1992.

[15] NISHIMURA, K. et al., Fusion Technol. **17** (1986) 86.

[16] KANEKO, O., KUBO, S., NISHIMURA, K., SHOJI, T., HOSOKAWA, M., et al., Confinement characteristics of high power heated plasma in CHS, in *Plasma Physics and Controlled Fusion Research (Proc. 13th Int. Conf., Washington, DC, 1990), Vol. 2, IAEA, Vienna*, pages 473–481, 1991.

[17] OKAMURA, S. et al., Heating experiments using neutral beams with variable injection angles and ICRF waves in a compact helical system, in *Plasma Physics and Controlled Fusion Research (Proc. 14th Int. Conf., Würzburg, 1992), Vol. 1, IAEA, Vienna*, pages 277–290, 1993.

[18] FOWLER, R. H., MORRIS, R. N., ROME, J. A., and HANATANI, K., Nucl. Fusion **30** (1990) 997.

[19] HANATANI, K. et al., Nucl. Fusion **32** (1992) 1769.

[20] YAMADA, H. et al., Nucl. Fusion **32** (1992) 25.

[21] HIRSHMAN, S. P. et al., Comput. Phys. Commun. **43** (1986) 143.

[22] UO, K. et al., Studies on currentless Heliotron E plasmas. in *Plasma Physics and Controlled Fusion Research (Proc. 11th Int. Conf., Kyoto, 1986), Vol. 2 IAEA, Vienna*, page 355, 1987.

[23] MURAKAMI, M. et al., Bull. Am. Phys. Soc. **31** (1986) 1415.

[24] SANO, F. et al., Nucl. Fusion **30** (1990) 81.

[25] SATO, M., ZUSHI, H., SUDO, S., ITOH, K., NODA, N., et al., (1988) 470.

[26] ZUSHI, H. et al., Nucl. Fusion **28** (1988) 1801.

[27] OBIKI, T. et al., Confinement improvement in ECH and NBI heated HeliotronIE plasmas, in *Plasma Physics and Controlled Fusion Research (Proc. 13th Int. Conf., Washington, DC, 1990), Vol. 2, IAEA, Vienna*, page 425, 1991.

[28] W7-A Team, Ohmic heating in the W7-A stellarator, in *Plasma Physics and Controlled Fusion Research (Proc. 6th Int. Conf., Berchtesgaden, 1992), Vol. 2, IAEA, Vienna*, pages 81–93, 1977.

[29] W7-A Team, Neutral injection in the W7-A stellarator with reduced ohmic current, in *Plasma Physics and Controlled Fusion Research (Proc. 8th Int. Conf., Brussels,*

1980), Vol. 2, IAEA, Vienna, pages 185–197, 1981.

[30] WOBIG, H., MASSBERG. H., RENNER, H., et al., Plasma confinement in the W7-A stellarator, in *Plasma Physics and Controlled Fusion Research (Proc. 11th Int. Conf., Kyoto, 1986), Vol. 2, IAEA, Vienna*, pages 367–381, 1987.

[31] GRIEGER, G. and W7-A Team, Plasma Phys. Controlled Fusion **28** (1986) 43.

[32] RENNER, H. et al., Plasma Phys. Controlled Fusion **31** (1989) 1579.

[33] GRIEGER, G., LOTZ, W., MERKEL, P., NÜHRENBERG, J., SAPPER, J., et al., Phys. Fluids B **4** (1992) 2081.

[34] JÄNICKE, R., ASCASIBAR, E., GRIGULL, P., LAKICEVIC, I., WELLER, A., and ZIPPE, M., Nucl. Fusion **33** (1993) 687.

[35] STROTH, U., MURAKAMI, M., KÜHNER, G., MAASSBERG, H., and DORY, R. A., A first step to a Joint Stellarator Database, IPP Report III/195, Max-Planck-Institut für Plasmaphysik, Garching, F.R.G., 1994.

[36] RINGLER, H., GASPARINO, U., KÜHNER, G., MASSBERG, H., RENNER, H., et al., Plasma Phys. Controlled Fusion **32** (1990) 933.

[37] WAGNER, F. and STROTH, U., Plasma Phys. Controlled Fusion **35** (1993) 1321.

[38] MAASSBERG, H., BRAKEL, R., BURHENN, R., GASPARINO, U., GRIGULL, P., et al., Plasma Phys. Controlled Fusion **35** (1993) B319.

[39] HARTFUSS, H. J., ENDLER, M., ERCKMANN, V., GASPARINO, U., GIANNONE, L., et al., Plasma Phys. Controlled Fusion **36** (1994) B17.

[40] LISTER, G. G., POST, D. E., and GOLDSTON, R. J., Computer simulation of neutral beam injection into tokamaks using monte carlo techniques, in *Proceedings of the* 3^{rd} *Symp. of Plasma Heating in Toroidal Devices, Varenna, Italy*, pages 303–307, Editrice Compositori, Bologna, 1976.

[41] STROTH, U., BRANAS, B., ESTRADA, T., GIANNONE, L., HARTFUSS, H. J., HIRSCH, M., KICK, M., KÜHNER, G., SATTLER, S., BALDZUHN, J., BRAKEL, R., ERCKMANN, V., JÄNICKE, R., RINGLER, H., and WAGNER, F., Pysica Scripta **51** (1995) 655.

[42] CONNOR, J. W. and TAYLOR, J. B., Nucl. Fusion **17** (1977) 1047.

[43] ZARNSTORFF, M. C., BARNES, C. W., EFTHIMION, P. C., HAMMETT, G. W., HORTON, W., et al., Advances in transport understanding using perturbative techniques in TFTR, in *Plasma Physics and Controlled Fusion Research (Proc.* 13^{th} *Int. Conf., Washington, DC, 1990), Vol. 1, IAEA, Vienna*, page 109, 1991.

List of Tables

List of Figures

Device	R	a	τ_0	τ_a	$\tau_{2/3}$	N_{tot}	N_{Std}
ATF	2.04	0.27	0.26	1.00	0.59	237	232
CHS	0.94	0.20	0.31	1.10	0.54	197	197
Heliotron E	2.17	0.21	0.51	2.75	0.95	121	120
W7-A	2.05	0.09	0.35-0.52	0.35-0.52	0.35-0.52	13	13
W7-AS	2.00	0.11-0.18	0.33-0.54	0.33-0.54	0.33-0.54	291	250

Table 1: Parametric overview of the devices included in the database. The total number of contributed observations as well as the number of observation included in the standard set used in the regression analyses are given.

Device	heating	B_t				$\bar{n}_e$				P_{tot}				N_{Std}
	method	av.	min.	max.	dev.	av.	min.	max.	dev.	av.	min.	max.	dev.	
ATF	ECH	0.98	0.64	1.89	0.24	0.60	0.33	1.04	0.18	0.24	0.05	0.41	0.09	53
	NBI	1.02	0.45	1.91	0.37	5.23	1.31	11.0	1.86	0.80	0.27	1.48	0.26	127
	mixed	1.06	0.45	1.89	0.34	1.20	0.43	4.74	0.68	0.56	0.20	1.13	0.25	52
CHS	ECH	1.02	0.85	1.72	0.35	0.59	0.24	1.47	0.30	0.12	0.12	0.12	0.00	30
	NBI	0.75	0.44	1.46	0.29	3.97	0.72	7.90	1.64	0.60	0.06	0.94	0.24	167
Heliotron E	ECH	1.84	0.94	1.94	0.20	1.20	0.49	3.02	0.66	0.29	0.08	0.50	0.12	33
	NBI	1.60	0.94	1.90	0.44	5.15	1.22	11.5	2.91	1.38	0.14	2.89	0.77	87
W7-A	ECH	1.73	1.25	2.50	0.63	1.25	0.62	2.30	0.52	0.09	0.04	0.13	0.03	13
W7-AS	ECH	1.71	1.24	2.56	0.61	2.67	0.83	8.61	1.83	0.33	0.12	0.84	0.13	198
	NBI	1.30	1.24	2.53	0.27	8.66	2.43	18.5	4.10	0.50	0.18	1.18	0.31	45
	mixed	2.53	2.53	2.54	0.00	5.38	3.56	6.45	1.27	0.67	0.54	0.95	0.13	7

Table 2: Average, minimum, maximum values and the value of one standard deviation of the distribution of some plasma parameters for the different devices and heating methods. Only data from the standard set are included.

device		$\log a$	$\log P_{tot}$	$\log \bar{n}_e$	$\log B_t$	$\log \tau_{2/3}$
ATF	$\log P_{tot}$		1			
	$\log \bar{n}_e$		0.74	1		
	$\log B_t$		0.09	0.05	1	
CHS	$\log P_{tot}$		1			
	$\log \bar{n}_e$		0.95	1		
	$\log B_t$		-0.28	-0.26	1	
Heliotron E	$\log P_{tot}$		1			
	$\log \bar{n}_e$		0.84	1		
	$\log B_t$		-0.50	-0.52	1	
W7-AS	$\log a$	1				
	$\log P_{tot}$	-0.01	1			
	$\log \bar{n}_e$	-0.01	0.64	1		
	$\log B_t$	0.26	0.29	0.27	1	
	$\log \tau_{2/3}$	-0.03	-0.00	-0.09	0.45	1

Table 3: Correlation matrices of the standard set for the contributions from the individual devices.

Device	α_x	α_a	α_R	α_P	α_n	α_B	α_ι	rmse
ATF	-1.58±0.02	2.00	1	-0.59±0.03	0.51±0.02	0.77±0.05	0.00	0.099
CHS	-1.71±0.03	2.00	1	-0.89±0.04	0.72±0.04	0.89±0.03	0.00	0.063
Heliotron E	-1.50±0.03	2.00	1	-0.62±0.04	0.56±0.04	0.59±0.08	0.00	0.093
W7-AS	-1.02±0.09	2.21±0.09	1	-0.54±0.04	0.50±0.02	0.73±0.05	0.43±0.08	0.087

Table 4: Regression results for the individual devices from the standard set. Parameters constrained to a fixed value are underlined. The root-mean-square errors correspond to $\log_{10}$ values.

	Devices	N_{Std}	α_x	α_a	α_R	α_P	α_n	α_B	α_ι
1	W7-AS	250	-0.94±0.09	2.21±0.09	0.74	-0.54±0.04	0.50±0.02	0.73±0.05	0.43±0.08
2	W7-A/W7-AS	263	-0.90±0.08	2.27±0.07	0.74	-0.50±0.03	0.49±0.02	0.75±0.05	0.39±0.08
3	ATF/CHS	429	-1.53±0.01	2.00	0.81±0.03	−0.59	0.51	0.77	0.00
4	ATF/Heliotron E	352	-1.44±0.01	2.00	0.80	−0.59	0.51	0.77	0.36±0.05
5	ATF/CHS/Heliotron E	549	-1.40±0.17	2.06±0.20	0.74±0.11	-0.63±0.02	0.53±0.02	0.80±0.03	0.39±0.13
6	ATF/CHS/Heliotron E	549	-1.88±0.07	1.51±0.09	1.04±0.05	-0.62±0.02	0.53±0.02	0.81±0.03	0.00

Table 5: Regression analyses using subsets of the devices for the investigation of the dependences on a, R and ι. Constraint parameters are underlined.

	α_x	α_a	α_R	α_P	α_n	α_B	α_ι	α_s	rmse
1	-0.95±0.07	2.24±0.06	0.65±0.04	-0.59±0.02	0.51±0.01	0.81±0.02	0.42±0.05	-0.29±0.02	0.0905
2	-1.79±0.03	1.65±0.04	0.98±0.03	-0.60±0.02	0.53±0.01	0.91±0.02	-0.10±0.03	0	0.0981
3	-0.98±0.06	2.21±0.05	0.65	-0.59±0.02	0.51±0.01	0.83±0.02	0.40±0.05	-0.28±0.02	0.0905
4	-1.10±0.07	2.17±0.06	0.69±0.04	-0.60±0.02	0.51±0.01	0.81±0.02	0.41±0.05	-0.21±0.02	0.0898
5	-1.31±0.06	2.06±0.06	0.74±0.04	-0.61±0.02	0.52±0.01	0.81±0.02	0.38±0.05	-0.08±0.02	0.0899

Table 6: Regression analyses under different assumptions of the entire standard set with 812 observations. 1: unconstrained fit, 2: constrained α_s, 3: dimensionally correct fit, 4: assume 15% shorter τ_E for W7-AS, 5: assume 20% larger a for W7-AS. Constrained values are underlined.

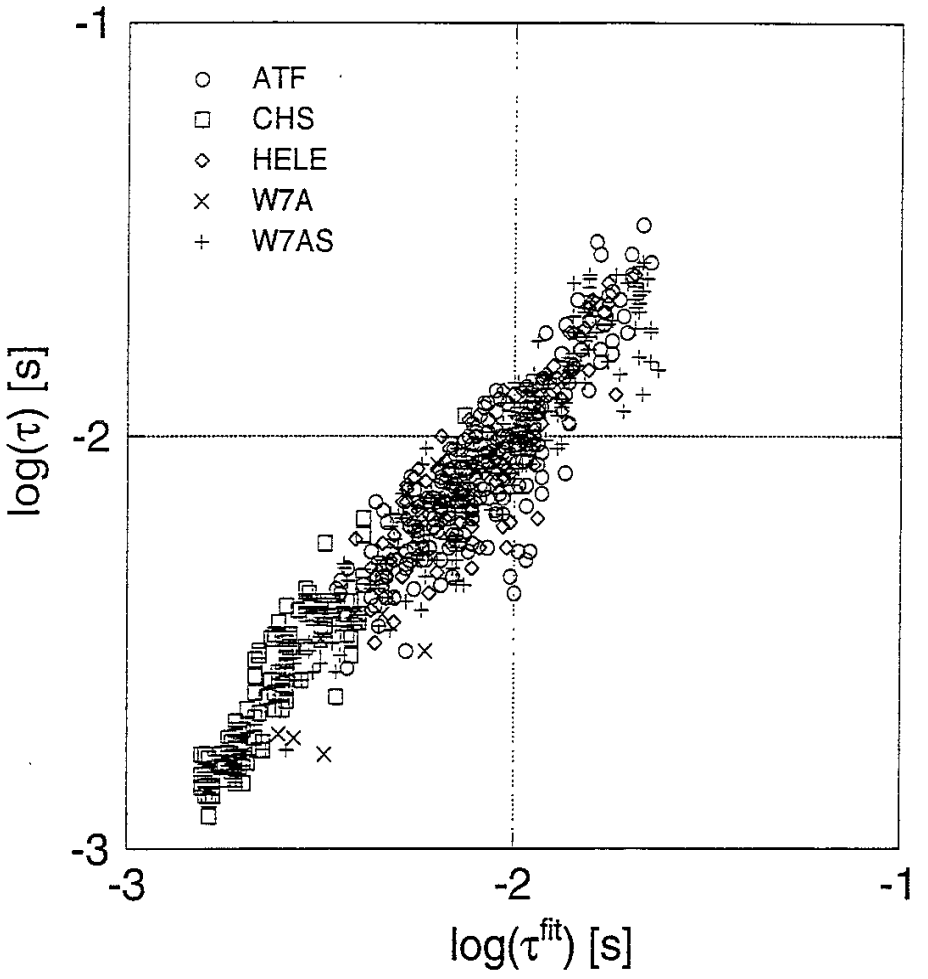

Figure 1: Confinement times of the entire standard set compared with the best fit from Tab. 6 ,(no. 1).

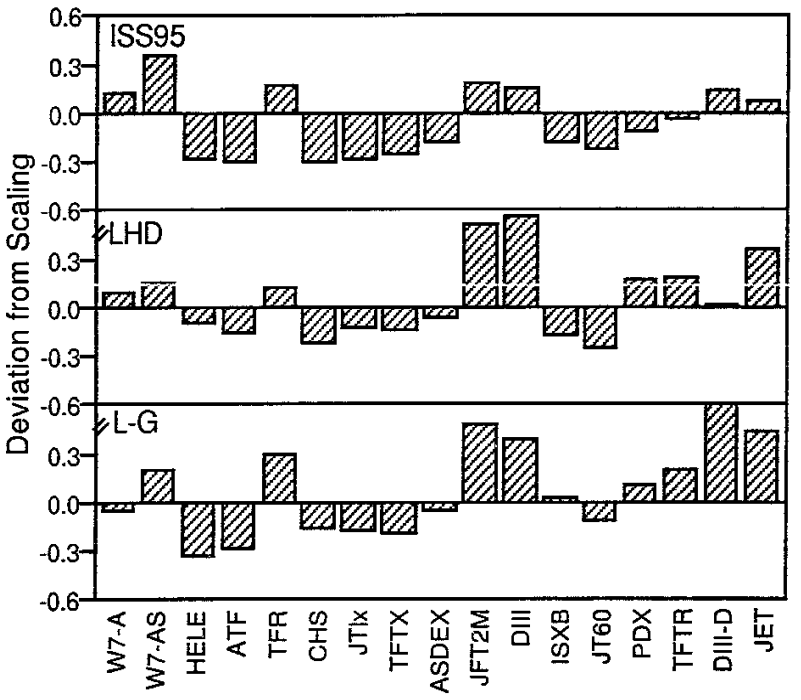

Figure 2: $(\tau_E - \tau^{scal})/\tau^{scal}$ averaged over all discharges of each stellarator from this database and each tokamak from the ITER L mode database. For τ^{scal} the predictions from the scaling expressions ISS95, LHD and L-G are used. The devices are ordered by ascending inverse aspect ratio. JTlx refers to JT60 with lower x-point and TFTX to aspect-ratio experiments in TFTR.

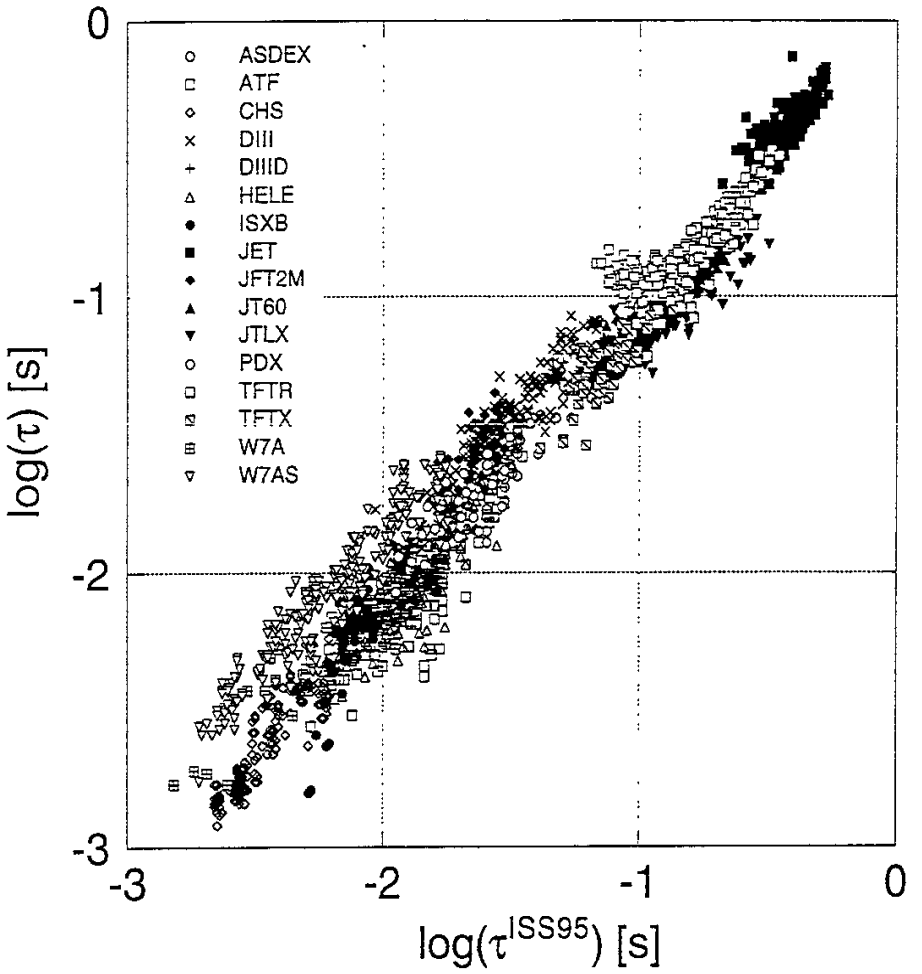

Figure 3: τ_E versus the prediction from the ISS95 expression (Tab. 6 , no. 3) for this database and tokamaks from the ITER L mode database.

Recent Issues of NIFS Series

NIFS-327 Y. Hamada, A. Nishizawa, Y. Kawasumi, K. Kawahata, K. Itoh, A. Ejiri, K. Toi, K. Narihara, K. Sato, T. Seki, H. Iguchi, A. Fujisawa, K. Adachi, S. Hidekuma, S. Hirokura, K. Ida, M. Kojima, J. Koong, R. Kumazawa, H. Kuramoto, R. Liang, T. Minami, H. Sakakita, M. Sasao, K.N. Sato, T. Tsuzuki, J. Xu, I. Yamada, T. Watari,
Fast Potential Change in Sawteeth in JIPP T-IIU Tokamak Plasmas; Dec. 1994

NIFS-328 V.D. Pustovitov,
Effect of Satellite Helical Harmonics on the Stellarator Configuration; Dec. 1994

NIFS-329 K. Itoh, S-I. Itoh and A. Fukuyama,
A Model of Sawtooth Based on the Transport Catastrophe; Dec. 1994

NIFS-330 K. Nagasaki, A. Ejiri,
Launching Conditions for Electron Cyclotron Heating in a Sheared Magnetic Field; Jan. 1995

NIFS-331 T.H. Watanabe, Y. Todo, R. Horiuchi, K. Watanabe, T. Sato,
An Advanced Electrostatic Particle Simulation Algorithm for Implicit Time Integration; Jan. 1995

NIFS-332 N. Bekki and T. Karakisawa,
Bifurcations from Periodic Solution in a Simplified Model of Two-dimensional Magnetoconvection; Jan. 1995

NIFS-333 K. Itoh, S.-I. Itoh, M. Yagi, A. Fukuyama,
Theory of Anomalous Transport in Reverse Field Pinch; Jan. 1995

NIFS-334 K. Nagasaki, A. Isayama and A. Ejiri
Application of Grating Polarizer to 106.4GHz ECH System on Heliotron-E; Jan. 1995

NIFS-335 H. Takamaru, T. Sato, R. Horiuchi, K. Watanabe and Complexity Simulation Group,
A Self-Consistent Open Boundary Model for Particle Simulation in Plasmas; Feb. 1995

NIFS-336 B.B. Kadomtsev,
Quantum Telegragh : is it possible?; Feb. 1995

NIFS-337 B.B.Kadomtsev,
Ball Lightning as Self-Organization Phenomenon; Feb. 1995

NIFS-338 Y. Takeiri, A. Ando, O. Kaneko, Y. Oka, K. Tsumori, R. Akiyama, E. Asano, T.

Kawamoto, M. Tanaka and T. Kuroda,
High-Energy Acceleration of an Intense Negative Ion Beam; Feb. 1995

NIFS-339 K. Toi, T. Morisaki, S. Sakakibara, S. Ohdachi, T.Minami, S. Morita, H. Yamada, K. Tanaka, K. Ida, S. Okamura, A. Ejiri, H. Iguchi, K. Nishimura, K. Matsuoka, A. Ando, J. Xu, I. Yamada, K. Narihara, R. Akiyama, H. Idei, S. Kubo, T. Ozaki, C. Takahashi, K. Tsumori,
H-Mode Study in CHS; Feb. 1995

NIFS-340 T. Okada and H. Tazawa,
Filamentation Instability in a Light Ion Beam-plasma System with External Magnetic Field; Feb. 1995

NIFS-341 T. Watanbe, G. Gnudi,
A New Algorithm for Differential-Algebraic Equations Based on HIDM; Feb. 13, 1995

NIFS-342 Y. Nejoh,
New Stationary Solutions of the Nonlinear Drift Wave Equation; Feb. 1995

NIFS-343 A. Ejiri, S. Sakakibara and K. Kawahata,
Signal Based Mixing Analysis for the Magnetohydrodynamic Mode Reconstruction from Homodyne Microwave Reflectometry; Mar.. 1995

NIFS-344 B.B.Kadomtsev, K. Itoh, S.-I. Itoh
Fast Change in Core Transport after L-H Transition; Mar. 1995

NIFS-345 W.X. Wang, M. Okamoto, N. Nakajima and S. Murakami,
An Accurate Nonlinear Monte Carlo Collision Operator; Mar. 1995

NIFS-346 S. Sasaki, S. Takamura, S. Masuzaki, S. Watanabe, T. Kato, K. Kadota,
Helium I Line Intensity Ratios in a Plasma for the Diagnostics of Fusion Edge Plasmas; Mar. 1995

NIFS-347 M. Osakabe,
Measurement of Neutron Energy on D-T Fusion Plasma Experiments; Apr. 1995

NIFS-348 M. Sita Janaki, M.R. Gupta and Brahmananda Dasgupta,
Adiabatic Electron Acceleration in a Cnoidal Wave; Apr. 1995

NIFS-349 J. Xu, K. Ida and J. Fujita,
A Note for Pitch Angle Measurement of Magnetic Field in a Toroidal Plasma Using Motional Stark Effect; Apr. 1995

NIFS-350 J. Uramoto,
Characteristics for Metal Plate Penetration of a Low Energy Negative Muonlike or Pionlike Particle Beam: Apr. 1995

NIFS-351 J. Uramoto,
An Estimation of Life Time for A Low Energy Negative Pionlike Particle Beam: Apr. 1995

NIFS-352 A. Taniike,
Energy Loss Mechanism of a Gold Ion Beam on a Tandem Acceleration System: May 1995

NIFS-353 A. Nishizawa, Y. Hamada, Y. Kawasumi and H. Iguchi,
Increase of Lifetime of Thallium Zeolite Ion Source for Single-Ended Accelerator: May 1995

NIFS-354 S. Murakami, N. Nakajima, S. Okamura and M. Okamoto,
Orbital Aspects of Reachable β Value in NBI Heated Heliotron/Torsatrons; May 1995

NIFS-355 H. Sugama and W. Horton,
Neoclassical and Anomalous Transport in Axisymmetric Toroidal Plasmas with Electrostatic Turbulence; May 1995

NIFS-356 N. Ohyabu
A New Boundary Control Scheme for Simultaneous Achievement of H-mode and Radiative Cooling (SHC Boundary); May 1995

NIFS-357 Y. Hamada, K.N. Sato, H. Sakakita, A. Nishizawa, Y. Kawasumi, R. Liang, K. Kawahata, A. Ejiri, K. Toi, K. Narihara, K. Sato, T. Seki, H. Iguchi, A. Fujisawa, K. Adachi, S. Hidekuma, S. Hirokura, K. Ida, M. Kojima, J. Koong, R. Kumazawa, H. Kuramoto, T. Minami,. M. Sasao, T. Tsuzuki, J.Xu, I. Yamada, and T. Watari,
Large Potential Change Induced by Pellet Injection in JIPP T-IIU Tokamak Plasmas; May 1995

NIFS-358 M. Ida and T. Yabe,
Implicit CIP (Cubic-Interpolated Propagation) Method in One Dimension; May 1995

NIFS-359 A. Kageyama, T. Sato and The Complexity Simulation Group,
Computer Has Solved A Historical Puzzle: Generation of Earth's Dipole Field; June 1995

NIFS-360 K. Itoh, S.-I. Itoh, M. Yagi and A. Fukuyama,
Dynamic Structure in Self-Sustained Turbulence; June 1995

NIFS-361 K. Kamada, H. Kinoshita and H. Takahashi,
Anomalous Heat Evolution of Deuteron Implanted Al on Electron Bombardment; June 1995

NIFS-362 V.D. Pustovitov,
Suppression of Pfirsch-schlüter Current by Vertical Magnetic Field in Stellarators; June 1995

NIFS-363 A. Ida, H. Sanuki and J. Todoroki
An Extended K-dV Equation for Nonlinear Magnetosonic Wave in a Multi-Ion Plasma; June 1995

NIFS-364 H. Sugama and W. Horton
Entropy Production and Onsager Symmetry in Neoclassical Transport Processes of Toroidal Plasmas; July 1995

NIFS-365 K. Itoh, S.-I. Itoh, A. Fukuyama and M. Yagi,
On the Minimum Circulating Power of Steady State Tokamaks; July 1995

NIFS-366 K. Itoh and Sanae-I. Itoh,
The Role of Electric Field in Confinement; July 1995

NIFS-367 F. Xiao and T. Yabe,
A Rational Function Based Scheme for Solving Advection Equation; July 1995

NIFS-368 Y. Takeiri, O. Kaneko, Y. Oka, K. Tsumori, E. Asano, R. Akiyama, T. Kawamoto and T. Kuroda,
Multi-Beamlet Focusing of Intense Negative Ion Beams by Aperture Displacement Technique; Aug. 1995

NIFS-369 A. Ando, Y. Takeiri, O. Kaneko, Y. Oka, K. Tsumori, E. Asano, T. Kawamoto, R. Akiyama and T. Kuroda,
Experiments of an Intense H- Ion Beam Acceleration; Aug. 1995

NIFS-370 M. Sasao, A. Taniike, I. Nomura, M. Wada, H. Yamaoka and M. Sato,
Development of Diagnostic Beams for Alpha Particle Measurement on ITER; Aug. 1995

NIFS-371 S. Yamaguchi, J. Yamamoto and O. Motojima;
A New Cable -in conduit Conductor Magnet with Insulated Strands; Sep. 1995

NIFS-372 H. Miura,
Enstrophy Generation in a Shock-Dominated Turbulence; Sep. 1995

NIFS-373 M. Natsir, A. Sagara, K. Tsuzuki, B. Tsuchiya, Y. Hasegawa, O. Motojima,
Control of Discharge Conditions to Reduce Hydrogen Content in Low Z Films Produced with DC Glow; Sep. 1995

NIFS-374 K. Tsuzuki, M. Natsir, N. Inoue, A. Sagara, N. Noda, O. Motojima, T. Mochizuki, I. Fujita, T. Hino and T. Yamashina,
Behavior of Hydrogen Atoms in Boron Films during H_2 and He Glow Discharge and Thermal Desorption; Sep. 1995